



Enhanced CO₂ capture in nitrogen-enriched microporous carbons derived from Polybenzoxazines containing azobenzene and carboxylic acid units

Mohamed Gamal Mohamed^{1,2} · Shymaa Mostafa Ebrahim¹ · Ahmed S. Hammam¹ · Shiao-Wei Kuo^{2,3} · Kamal I. Aly¹

Received: 6 March 2020 / Accepted: 1 July 2020 / Published online: 6 July 2020
© The Polymer Society, Taipei 2020

Abstract

In this study, we prepared nitrogen-doped microporous carbons (NMCs) from two different benzoxazine monomers (AMBZ, AEBZ), each containing both azobenzene and carboxylic groups, through a simple and environmentally friendly process of ring-opening polymerization (ROP), calcination, and KOH activation. We synthesized the AMBZ and AEBZ monomers through Mannich condensations of 4,4'-diaminodiphenylmethane (M) and 4,4'-diaminodiphenyl ether (E), respectively, with paraformaldehyde and 4-(4-hydroxyphenylazo)benzoic acid (Azo-COOH). Differential scanning calorimetry (DSC) revealed that the thermal curing temperatures of AMBZ and AEBZ (both ca. 230 °C) were lower than that of a typical Pa-type benzoxazine monomer (263 °C), suggesting that the azobenzene and COOH units acted as promoters and catalysts for the ROP of the benzoxazine units. In addition, after ROP of the benzoxazine units of AMBZ and AEBZ, the polymers PAMBZ and PAEBZ, respectively, displayed high glass transition temperatures (T_g) and high thermal stability, as evidenced using DSC and thermogravimetric analysis (TGA), due to their greater cross-linking densities. We used Brunauer–Emmett–Teller analysis, TGA, wide-angle X-ray diffraction, transmission electron microscopy, Raman spectroscopy, and X-ray photoelectron spectroscopy to examine the specific surface areas, porous structures, chemical compositions, and thermal stabilities of the resulting KOH-activated NMCs PAMBZ-A and PAEBZ-A. The CO₂ capture abilities and thermal properties of these two highly-nitrogen-doped microporous carbons, synthesized from polybenzoxazine (PBZ) resins containing azobenzene and COOH groups, were excellent when compared with those of other N-doped porous carbons derived from other PBZ matrices.

Keywords Benzoxazine · Ring-opening polymerization · Thermal stability · N-doped microporous carbon · CO₂ uptake

Electronic supplementary material The online version of this article (<https://doi.org/10.1007/s10965-020-02179-1>) contains supplementary material, which is available to authorized users.

- ✉ Mohamed Gamal Mohamed
mgamal.eldin12@yahoo.com
- ✉ Shiao-Wei Kuo
kuosw@faculty.nsysu.edu.tw
- ✉ Kamal I. Aly
kamalaly@aun.edu.eg

- ¹ Polymer Research Laboratory, Chemistry Department, Faculty of Science, Assiut University, Assiut 71516, Egypt
- ² Department of Materials and Optoelectronic Science, Center of Crystal Research, National Sun Yat-Sen University, Kaohsiung 804, Taiwan
- ³ Department of Medicinal and Applied Chemistry, Kaohsiung Medical University, Kaohsiung 807, Taiwan

Introduction

Carbon dioxide (CO₂) is the main greenhouse gas that contributes to anthropogenic global warming. Although wet cleaning with aqueous alkanolamine solutions is the chemical process employed most commonly for capturing CO₂, this method has several disadvantages, including high energy consumption, low efficiency, difficulties of renewal, equipment corrosion, solvent loss, and high cost [1–7]. The development of new and more effective strategies remains challenging, but it appears to be an urgent task for decreasing or capturing the amounts of CO₂ produced in various industrial processes. Porous organic polymers (POPs) have attracted much attention as porous materials for many applications, including sensors, removal of pollutants, CO₂ capture, storage and separation, drug delivery, catalysis, SO₂ adsorption, gene therapy, Li-S batteries, energy conversion, and light-harvesting; they

have several attractive properties: high surface areas, large porosities, large pore volumes, chemical resistance, biocompatibility, and excellent electrical conductivity [8–15]. Many methods—including thermal decomposition, chemical vapor deposition, condensation, reactions of melamine with porous carbon, and the carbonization and KOH activation of N-containing materials—have been used widely for the preparation of N-doped porous carbon materials (NMCs) having high surface areas and excellent porosities [16–26].

Polybenzoxazines (PBZs) are phenolic resin-derived, heterocyclic, high-performance thermosetting polymers that can be prepared through thermal ring-opening polymerization (ROP) of benzoxazine monomers [27–36]. The preparation of benzoxazine monomers can be performed readily through Mannich condensations of primary or aromatic amines, phenols, and paraformaldehyde in the presence or absence of a solvent [37–39]. PBZs have attracted interest from both industrial and academic fields because of their many useful properties: low surface energies, flame-retardance, high thermal stabilities, near-zero shrinkage upon polymerization, good solvent-resistance, excellent mechanical properties, low water absorption, low melt viscosities, hydrophobic surfaces, high carbon residue rates, low dielectric constants, corrosion resistance, ease of processability, no release of volatile products, high glass transition temperatures (T_g), and highly flexible molecular design [40–46]. The properties of PBZs have also been improved through (i) the use of benzoxazines monomers containing reactive functional groups (e.g., propargyl, nitrile, hydroxyalkyl) and (ii) incorporation, copolymerization, or blending of the benzoxazine monomers with polyhedral oligomeric silsesquioxane (POSS), carbon nanotubes, nano clay, polydimethylsiloxane (PDMS), or graphene [47–50].

Recently, PBZ resins have been used as precursors for the preparation of high-performance nitrogen-doped carbon materials (NMCs) for CO₂ adsorption and energy storage, because their higher contents of N and O atoms inside the carbon matrix after thermal curing polymerization, carbonization, and activation can enhance their affinity toward CO₂ [51, 52]. For example, we have previously reported that BZCN-A, microporous carbon derived from a nitrile-functionalized benzoxazine matrix, is a porous material of high surface area and exhibiting a CO₂ uptake of 2.82 mmol g⁻¹ [53]. Li et al. prepared the nitrogen-containing porous carbon NPC-1 through thermal curing polymerization, calcination, and KOH chemical activation of a nitrile-functionalized benzoxazine monomer and a soft templating agent (surfactant F127) [54]. They found that NPC-1 exhibited high CO₂ uptakes of 6.20 and 3.95 mmol g⁻¹ at 0 and 25 °C, respectively. Furthermore, Hao et al. synthesized nitrogen-containing porous carbon monoliths from poly(benzoxazine-co-resol) polymers as carbon precursors; these materials possessed interconnected meso-/macropore structured and displayed outstanding CO₂ uptake [55].

Herein, we describe two new benzoxazine monomers containing both azobenzene and COOH groups (AMBZ and AEBZ), prepared through Mannich condensation (Scheme 1). Fourier transform infrared (FTIR) spectroscopy, nuclear magnetic resonance (NMR) spectroscopy, thermogravimetric analysis (TGA), and differential scanning calorimetry (DSC) revealed their thermal curing behavior, thermal properties, and chemical structures. We then used wide-angle X-ray diffraction (WXR), X-ray photoelectron spectroscopy (XPS), transmission electron microscopy (TEM), Raman spectroscopy, and N₂ adsorption/desorption and CO₂ adsorption measurements to examine the properties of the microporous carbon materials PAMBZ-A and PAEBZ-A derived from AMBZ and AEBZ, respectively, including their thermal stabilities, textural properties [e.g., Brunauer–Emmett–Teller (BET) surface areas and pore-size distributions], chemical compositions, and CO₂ uptake abilities. We found that the incorporation of both azobenzene and COOH groups into the PBZ matrices had a great effect on the properties of the resulting N-doped carbon materials—in particular, it enhanced their CO₂ capture abilities.

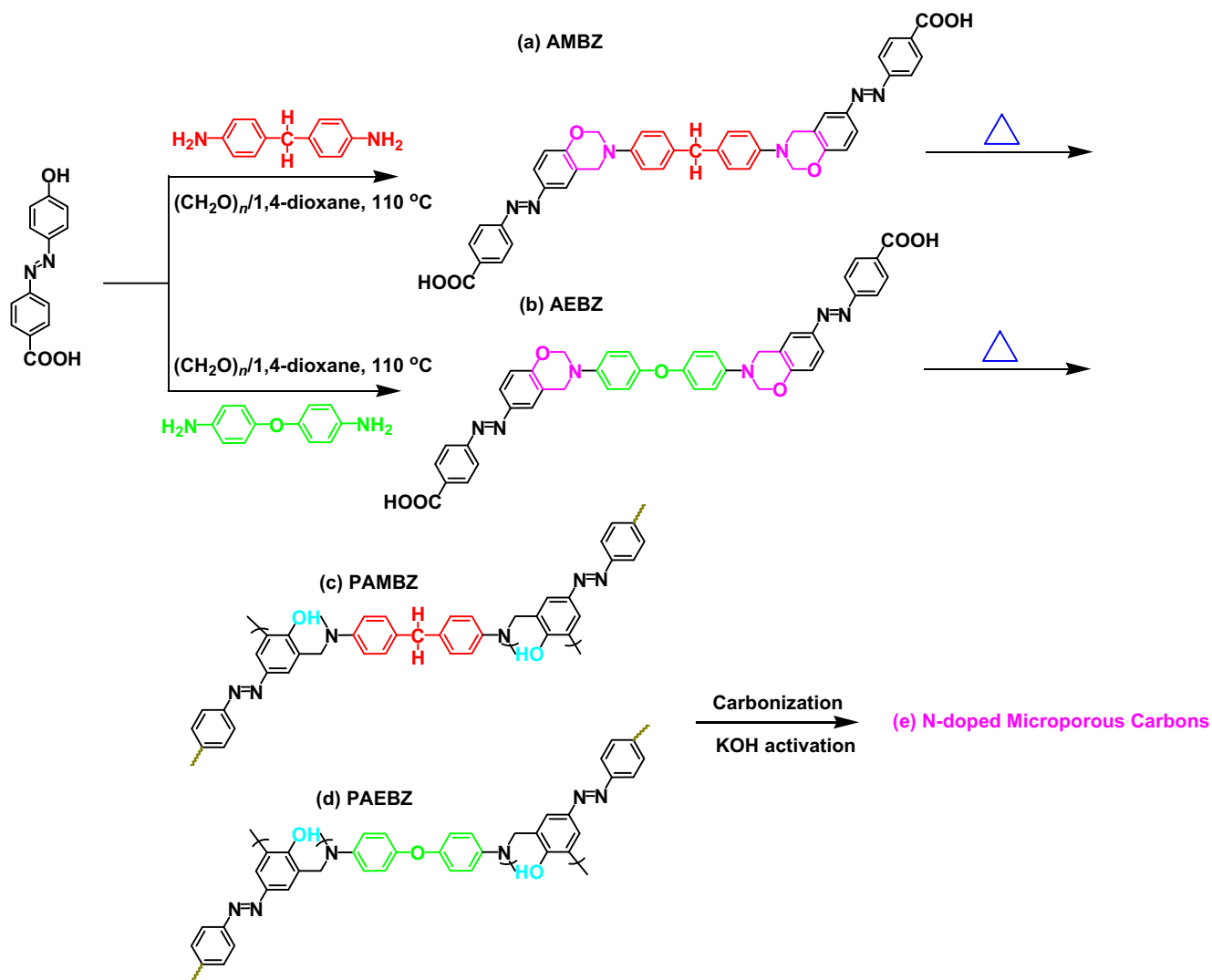
Experimental section

Materials

4-Aminobenzoic acid, anhydrous magnesium sulfate (MgSO₄), sodium hydroxide (NaOH), methanol (MeOH), sodium nitrite (NaNO₂), potassium hydroxide (KOH), 4,4'-diamino diphenylmethane, 4,4'-diaminodiphenyl ether, phenol, paraformaldehyde (CH₂O)_n, tetrahydrofuran (THF), 1,4-dioxane, HCl solution (37%), and ethyl acetate (EA) were purchased from Acros.

4-(4-Hydroxyphenylazo)benzoic acid (Azo-COOH) [47] (Scheme S1)

A solution of sodium nitrite (6.90 g, 0.100 mmol) in water (20 mL) was added dropwise to a stirred solution of 4-aminobenzoic acid (13.7 g, 0.100 mmol) in dilute HCl (40 mL) at 0 °C and then the mixture was diluted with cold MeOH (300 mL). A cooled solution of phenol (9.41 g, 0.100 mmol), NaOH (10.8 g, 0.190 mmol), and MeOH (50 mL) were added to this solution. After stirring for 2 h, dilute HCl (0.5 N) was added into the mixture to afford Azo-COOH as a red powder (9.00 g, 66%); m.p.: 273–275 °C (DSC). FTIR (KBr, cm⁻¹): 3463–3204 (OH), 3053–2500 (COOH), 1660 (C=O). ¹H NMR (500 MHz, DMSO-*d*₆, δ , ppm): 6.88–8.12 (m, 8H, ArH), 10.17 (s, 1H, OH), 13.13 (s, 1H, COOH). ¹³C NMR (125 MHz, DMSO-*d*₆, δ , ppm): 168 (C=O).



Scheme 1 Synthesis of (e) NMCs from (a) AMBZ, (b) AEBZ, (c) PAMBZ, and (d) PAEBZ through ROP, carbonization, and KOH chemical activation

4,4'-(((Methylenebis(4,1-phenylene))bis(3,4-dihydro-2H-benzo[e][1,3]oxazine-3,7-diyl))bis(diazene-2,1-diyl))dibenzoic acid (AMBZ)

In a round-bottom flask (100 mL) equipped with a condenser and a magnetic stirrer, a solution of 4,4'-diaminodiphenylmethane (1.00 g, 5.07 mmol), paraformaldehyde (0.61 g, 20.2 mmol), and Azo-COOH (2.44 g, 10.1 mmol) in 1,4-dioxane (50 mL) was heated under reflux at 110 °C for 24 h under a N_2 atmosphere. The mixture was cooled to room temperature and the 1,4-dioxane was evaporated under reduced pressure at 50 °C. A small amount of THF was added to the residue; the AMBZ monomer was precipitated from hexane (300 mL) as an orange solid (3.00 g, 82%). FTIR (KBr, cm^{-1}): 3053–2500 (COOH), 1666 (C=O), 1602 (C=C), 1230 (C–O–C asymmetric stretching), 933 (benzoxazine-related band). ^1H NMR (500 MHz, $\text{DMSO}-d_6$,

δ , ppm): 13.13 (s, 2H, COOH), 7.99–6.04 (m, C-H aromatic), 5.52 (s, 4H, OCH_2N), 4.73 (s, 4H, ArCH_2N), (s, 2H, ArCH_2Ar). ^{13}C NMR (125 MHz, $\text{DMSO}-d_6$, δ , ppm): 168 (C=O), 161.81–113.54 (aromatic), 80.35 (OCH_2N), 66.72 (ArCH_2Ar), 49.01 (ArCH_2N).

4,4'-(((Oxybis(4,1-phenylene))bis(3,4-dihydro-2H-benzo[e][1,3]oxazine-3,7-diyl))bis(diazene-2,1-diyl))dibenzoic acid (AEBZ)

A solution of 4,4'-diaminodiphenyl ether (1.00 g, 5.00 mmol), paraformaldehyde (0.60 g, 20.00 mmol) and Azo-COOH (2.42 g, 10.0 mmol) in 1,4-dioxane (50 mL) was heated at 110 °C for 24 h under a N_2 atmosphere. The mixture was cooled to room temperature and the solvent was evaporated under reduced

pressure. A small amount of THF was added to the residue; AEBZ was precipitated from hexane (300 mL) to afford an orange solid (3.20 g, 87%). FTIR (KBr, cm^{-1}): 3053–2500 (COOH), 1690 (C=O), 1597 (C=C), 1228 (C–O–C asymmetric stretching), and 928 (benzoxazine-related band). ^1H NMR (500 MHz, $\text{DMSO-}d_6$, δ , ppm): 13.13 (s, 2H, COOH), 7.82–6.06 ((m, C-H aromatic), 5.51(s, 4H, OCH_2N), 4.74(s, 4H, ArCH_2N). ^{13}C NMR (125 MHz, $\text{DMSO-}d_6$, δ , ppm): 168 (C=O), 162.93–113.12 (aromatic), 80.63 (OCH_2N), 49.41 (ArCH_2N).

PAMBZ and PAEBZ

A desired amount of the AMBZ or AEBZ monomer was cured in an oven at various temperatures (110, 150, 180, 210, and 250 °C; for 2 h at each temperature) to afford a black powder.

NMCs derived from AMBZ and AEBZ

The desired amount of the AMBZ (AEBZ) monomer was polymerized in an oven for 5 h at 250 °C. The sample was then calcined in a tubular furnace (heating rate: 5 °C min^{-1}) under a N_2 atmosphere at 600 °C for 2 h to give PAMBZ-C (PAEBZ-C). The black sample was mixed with an aqueous KOH solution and stirred overnight. The water was evaporated under reduced pressure at 120 °C for 24 h. The activated sample was transferred to a tubular furnace (heating rate: 5 °C min^{-1}) and heated under a N_2 atmosphere at 800 °C for 8 h to afford PAMBZ-A (PAEBZ-A).

Results and discussion

Synthesis of AMBZ, AEBZ, PAMBZ, and PAMBZ

We prepared the AMBZ and AEBZ monomers through one-pot Mannich condensations, as displayed in Scheme 1. ^1H and ^{13}C NMR and FTIR spectroscopy confirmed their structures. Figure 1 presents the FTIR spectra of Azo-COOH, AMBZ, and PAMBZ. The spectrum of Azo-COOH (Fig. 1a) displays major absorption bands at 3470 and 3540 cm^{-1} corresponding to hydrogen-bonded and free OH groups; at 3050–2520 cm^{-1} for the hydrogen-bonded COOH dimer; and at 1666 cm^{-1} for C=O stretching. In the spectrum of the AMBZ monomer (Fig. 1b), characteristic absorption bands appeared at 3050–2520, 1666, 1230, and 933 cm^{-1} , representing the hydrogen-bonded COOH dimer, C=O stretching, asymmetric C–O–C stretching, and a benzoxazine-related band, respectively, but the signal for the OH unit was absent. After thermal treatment at 250 °C, the spectrum of PAMBZ (Fig. 1c) did not feature the characteristic signals for the asymmetric C–O–C stretching or the benzoxazine-related band. Figure 2 displays the FTIR spectra of Azo-COOH, AEBZ, and PAEBZ, recorded at room temperature. The spectrum of AEBZ (Fig. 2b) features characteristic absorption signals centered at 1690, 1228, and 928 cm^{-1} , corresponding to the C=O group, asymmetric C–O–C stretching, and out-of-plane C–H bending of the benzene ring, respectively. The characteristic signals at 1228 and 928 cm^{-1} related to the oxazine ring in AEBZ disappeared after its thermal curing polymerization at 250 °C to give PAEBZ (Fig. 2c). Figure 3 presents the ^1H NMR spectra of Azo-COOH, AMBZ, and AEBZ in $\text{DMSO-}d_6$. In the spectrum of Azo-COOH (Fig. 3a), signals appeared at 13.13 ppm for the COOH group, 10.47 ppm for the OH unit, and 6.97–

Fig. 1 FTIR spectra of (a) Azo-COOH, (b) AMBZ, and (c) PAMBZ

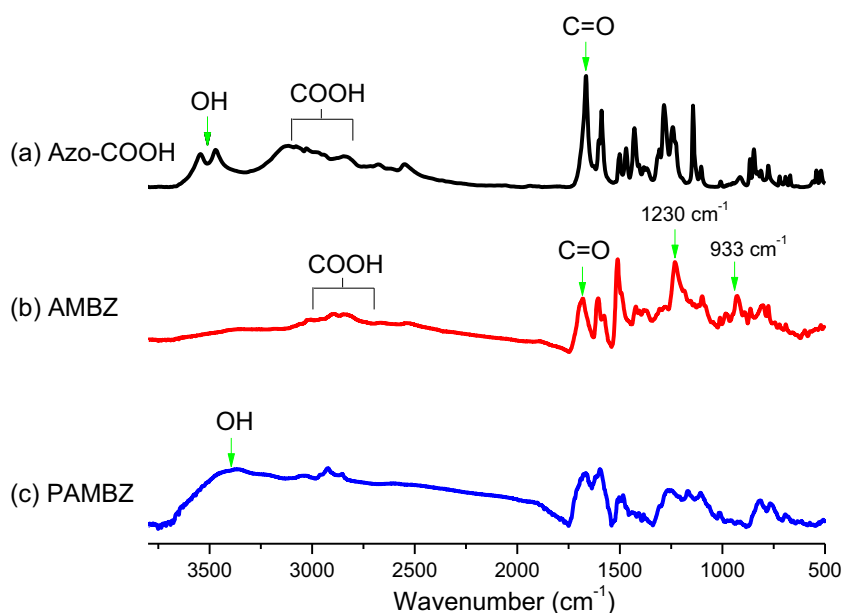
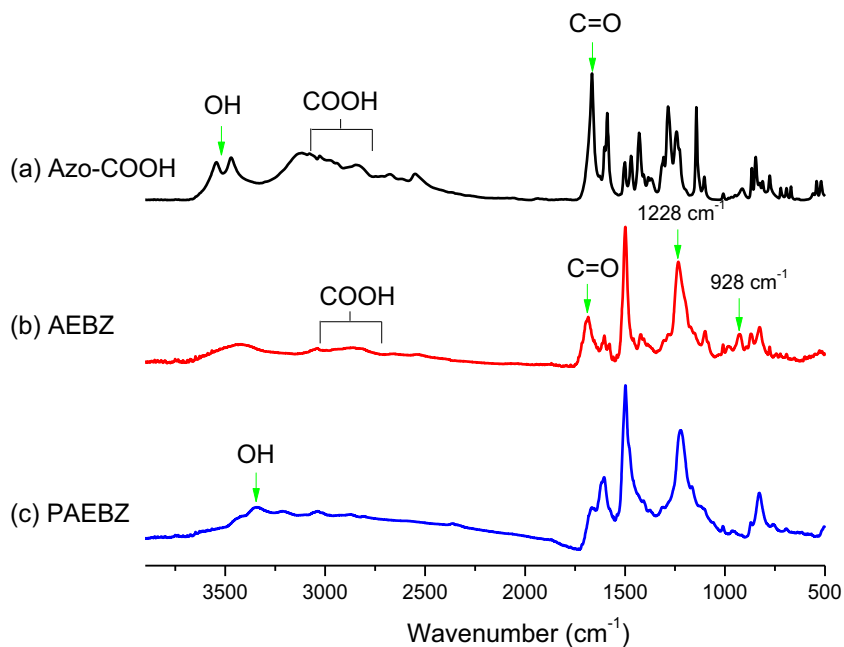


Fig. 2 FTIR spectra of (a) Azo-COOH, (b) AEBZ, and (c) PAEBZ



8.10 ppm for the aromatic protons. The spectra of AMBZ (Fig. 3b) and AEBZ (Fig. 3c) feature peaks at 13.13, 4.73, and 5.52 ppm and at 13.13, 4.72, and 5.52 ppm, respectively, representing their COOH groups and the ArCH₂N and OCH₂N units of their oxazine rings, respectively. Also, the spectrum of AMBZ features a signal at 3.60 ppm for the methylene group (CH₂). Figure 4 provides the ¹³C NMR spectra of Azo-COOH, AMBZ, and AEBZ. The spectrum of Azo-COOH (Fig. 4a) features signals in the range 116.6–162.3 ppm for the azobenzene moiety and at

167.2 ppm for the C=O group. In the spectrum of AMBZ (Fig. 4b), signals appeared at 80.35, 66.72, and 49.01 ppm for the OCH₂N, ArCH₂N, and ArCH₂Ar units, respectively. The same characteristic signals appeared for the OCH₂N and ArCH₂N units in the spectrum of AEBZ (Fig. 4c), at 80.63 and 49.41 ppm, respectively, in addition to signals for the aromatic carbon nuclei in the range 158.54–113.11 ppm. Thus, the NMR and FTIR spectra confirmed the successful syntheses of Azo-COOH and the monomers AMBZ and AEBZ.

Fig. 3 ¹H NMR spectra of (a) Azo-COOH, (b) AMBZ, and (c) AEBZ

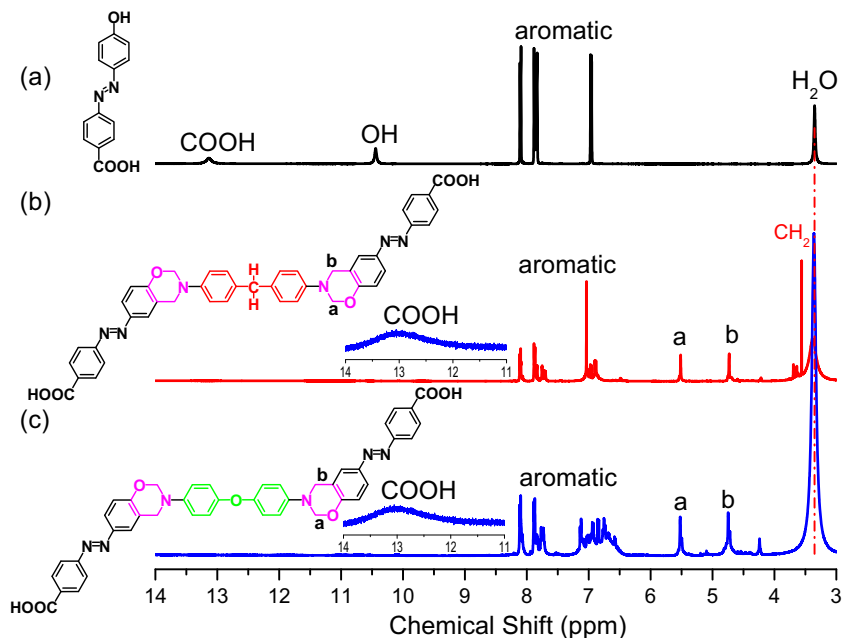
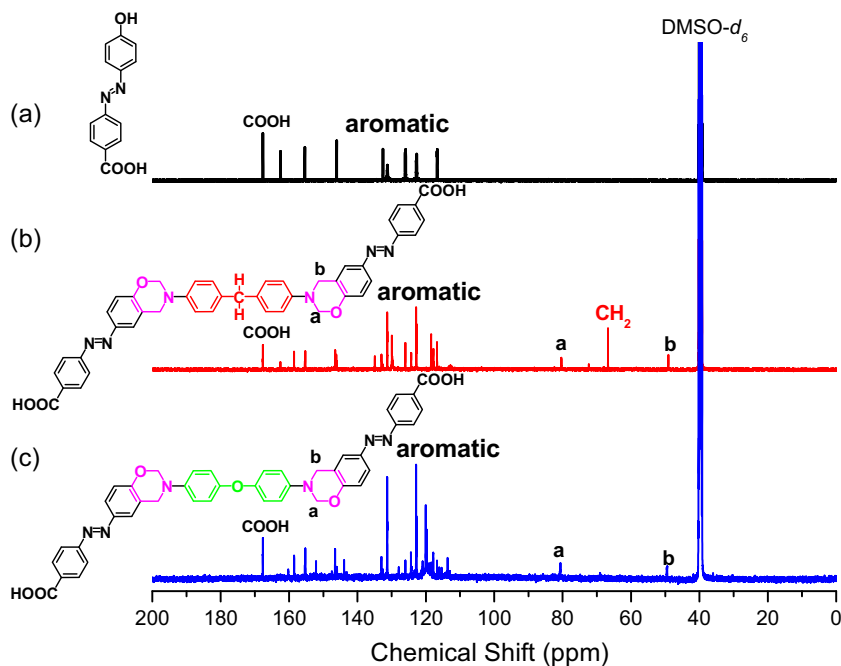


Fig. 4 ^{13}C NMR spectra of (a) Azo-COOH, (b) AMBZ and (c) AEBZ



Thermal curing polymerization of the monomers AMBZ and AEBZ

We used DSC and FTIR to study the thermal curing behavior of AMBZ and AEBZ. Figure 5 displays DSC profiles of the uncured AMBZ and after its polymerization at temperatures from 110 to 250 °C. The uncured AMBZ provided a maximum exothermic curing peak at 233 °C with a reaction heat of 291 J g⁻¹. After thermal polymerization of AMBZ at 110, 150,

and 180 °C, the maximum exothermic curing peaks appeared at 233, 232, and 244 °C, respectively, with reaction heats of 291, 250, and 237 J g⁻¹, respectively. Further thermal curing at temperatures from 210 to 250 °C resulted in the maximum exothermic curing peak of AMBZ disappearing completely; a glass transition temperature (T_g) of 236 °C appeared after thermal treatment at 210 °C, indicating complete ROP of the oxazine units and the formation of PAMBZ with high crosslinking density. After thermal treatment of AMBZ from

Fig. 5 (a) DSC thermograms and (b) FTIR spectra of the monomer AMBZ before and after curing at various temperatures

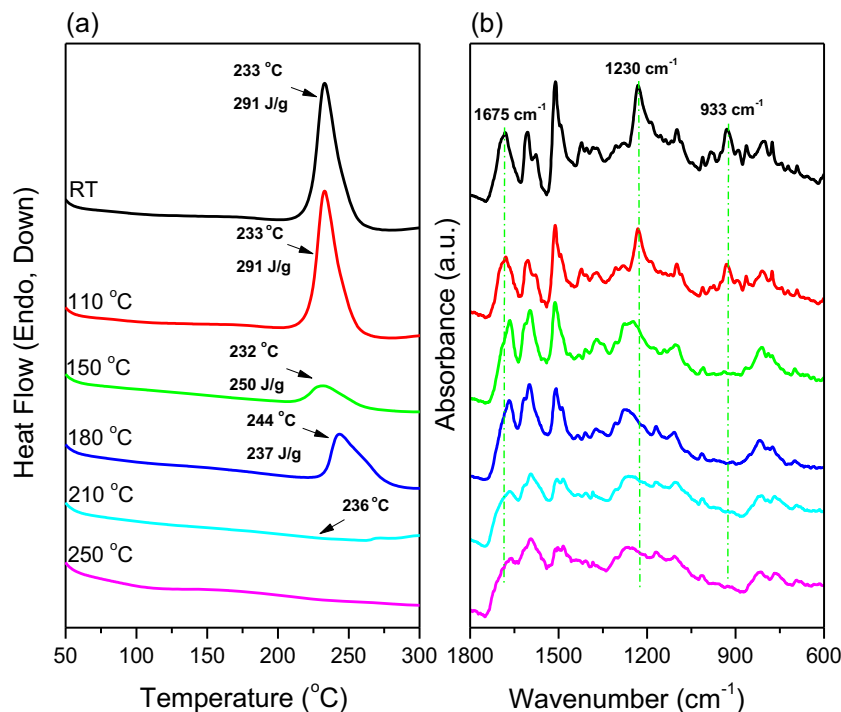
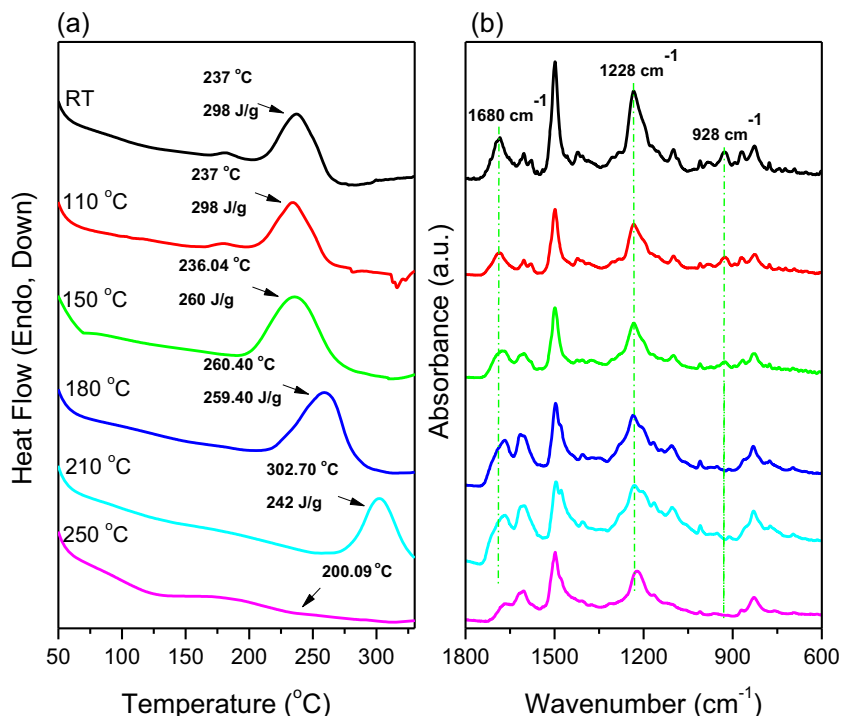


Fig. 6 **(a)** DSC thermograms and **(b)** FTIR spectra of the monomer AEBZ before and after curing at various temperatures



room temperature to 180 °C, the FTIR spectra featured absorption signals of the benzoxazine unit of AMBZ at 1230 and 933 cm^{-1} , representing the C–O–C unit and the benzoxazine mode, respectively (Fig. 5b). Further curing to 250 °C, however, resulted in complete disappearance of these characteristic absorption signals of the benzoxazine ring structure of the monomer. Figure 6a presents the DSC thermogram of AEBZ, featuring an exothermic peak at 237 °C and an enthalpy of

298 J g^{-1} . After thermal curing at temperatures of 110, 150, 180, and 210 °C, thermal curing peaks appeared at 237, 236, 260, and 302 °C, respectively, with reaction heats of 298, 260, 259, and 242 J g^{-1} , respectively. PAEBZ exhibited a glass transition temperature at 200 °C after thermal curing at 250 °C. More interestingly, the exothermic curing peaks for the oxazine units in AMBZ and AEBZ (Figs. 5a and 6a) were at lower temperatures than that of the typical Pa-type

Fig. 7 TGA profiles of the monomers **(a)** AMBZ and **(b)** AEBZ before and after curing at various temperatures

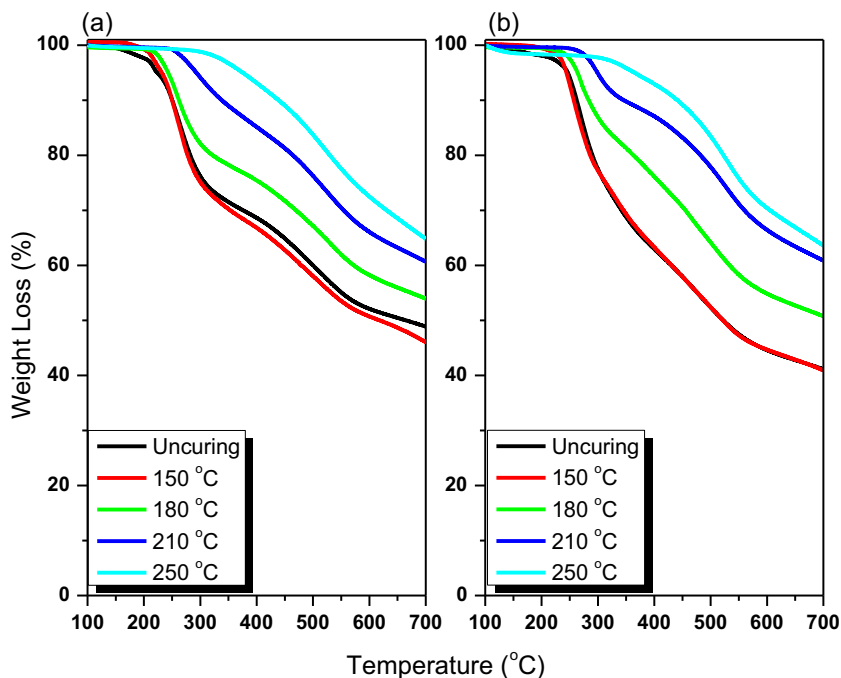


Table 1 Thermal stabilities, XPS analytical data, surface areas, and CO₂ uptake abilities of various samples

Samples	T_{d10} (°C)	Char yield (wt%)	XPS analysis (%)			S_{BET} (m ² g ⁻¹)	CO ₂ uptake (mmol g ⁻¹)	
			C	O	N		298 K	273 K
AMBZ	249	46	—	—	—	—	—	—
AEBZ	263	38	—	—	—	—	—	—
PAMBZ	426	58	—	—	—	—	—	—
PAEBZ	418	57	—	—	—	—	—	—
PAMBZ-A	—	—	81.2	16.5	2.3	462	3.63	5.53
PAEBZ-A	—	—	75.8	20.0	4.2	960	4.60	7.20

benzoxazine monomer (263 °C), presumably because the carboxylic acid and azobenzene units in AMBZ and AEBZ acted as catalysts for ROP of the benzoxazine unit [46]. Similarly, the characteristic absorption signals for the benzoxazine unit in the FTIR spectrum of AEBZ disappeared completely after its thermal treatment at 250 °C (Fig. 6b), consistent with the DSC behavior. The absorption intensity of the C=O unit of the COOH group decreased after increasing the thermal curing temperature to 180 or 250 °C for both AMBZ and AEBZ, due to the thermal polymerization of these two monomers and partial decarboxylation [46]. Furthermore, we used TGA under a N₂ atmosphere to examine the thermal stability of the uncured AMBZ and AEBZ and the products of their polymerizations after thermal curing at various temperatures (110–250 °C) (Fig. 7, Table 1). The uncured AMBZ and AEBZ exhibited decomposition temperatures (T_{d10}) of 249 and 263 °C, respectively, and char yields of 46 and 38 wt%,

respectively. The thermal decomposition temperatures and char yields of the PBZ matrices obtained after the polymerizations of AMBZ and AEBZ at 250 °C increased to 426 °C and 58 wt% and to 418 °C and 57 wt%, respectively, presumably because they had highly crosslinked structures arising from hydrogen bonding among the COOH groups or because of additional crosslinking arising from partial decarboxylation at 250 °C [46].

Characterization of NMCs derived from PAMBZ and PAEBZ

We performed N₂ adsorption/desorption measurements at 77 K to determine the porosity properties of the NMCs derived from AMBZ and AEBZ (Scheme 1(e)), including their BET surface areas, pore volumes, and pore size distributions (Fig. 8). The N₂ adsorption/desorption isothermal curves of PAMBZ-A and PAEBZ-A both featured type-I isotherms with rapid increases at low values of P/P_0 (<0.05), indicating that both NMCs were microporous carbon materials. The BET surface areas and total pore volumes were 464 m² g⁻¹ and

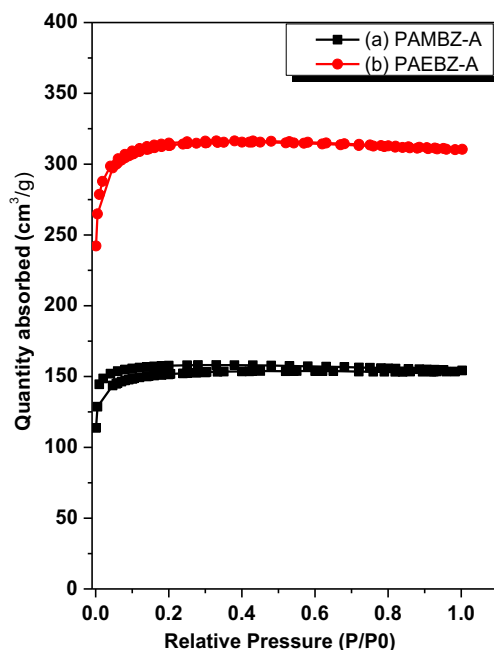
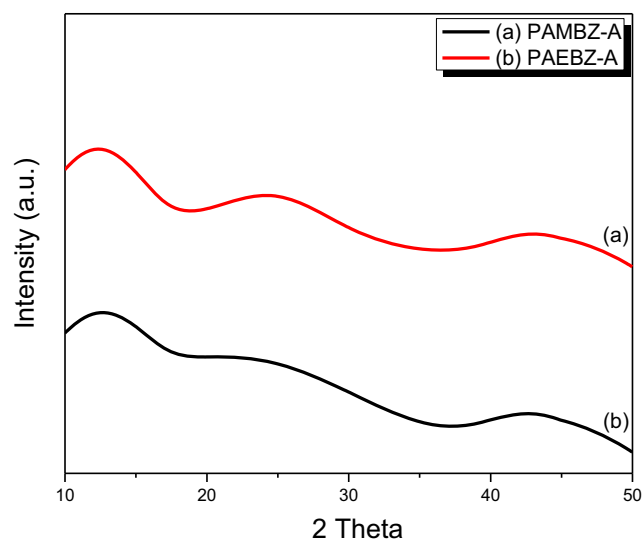
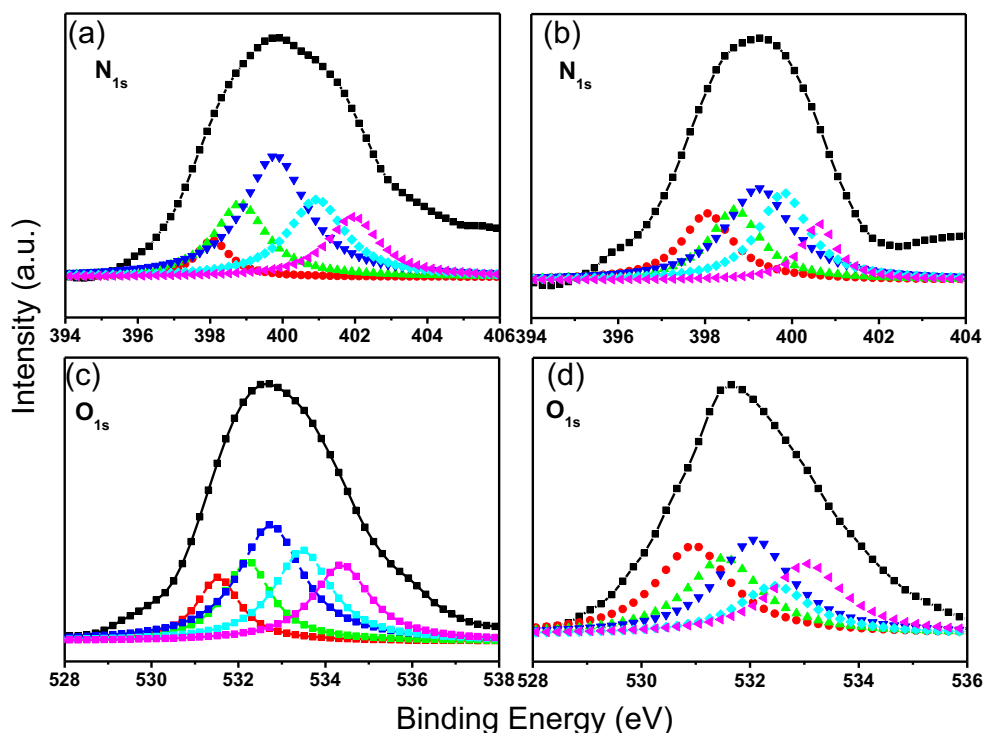
**Fig. 8** N₂ adsorption/desorption of PAMBZ-A and PAEBZ-A at 77 K**Fig. 9** WXR D spectra of PAMBZ-A and PAEBZ-A

Fig. 10 XPS results of PAMBZ-A (a, c) and PAEBZ-A (b, d)



0.204 cm³ g⁻¹, respectively, for PAMBZ-A and 960 m² g⁻¹ and 0.43 cm³ g⁻¹, respectively, for PAEBZ-A. We used non-local density functional theory to calculate average pore sizes in PAMBZ-A and PAEBZ-A (Fig. S1) of approximately 2.70 nm. TEM images revealed that, after KOH activation, PAMBZ-A and PAEBZ-A featured abundances of micropores in their structures (Fig. S2). Figure 9 displays powder XRD profiles of PAMBZ-A and PAEBZ-A, recorded at room temperature. Three broad diffraction peaks appeared at values of 2θ of 12.5° and 25° for the (002) plane, which represents irregular and amorphous carbon atoms, and 44° for the (100) plane, which represents graphitic carbon atoms [7]. Figure 10 displays the fitting spectra for N and O atoms on the surfaces of PAMBZ-A and PAEBZ-A, determined from the XPS data. The traces of both PAMBZ-A and PAEBZ-A revealed four types of N-containing species: pyridonic or pyridone N atoms (ca. 400 eV), quaternary N atoms (ca. 401 eV), pyridinic N atoms (ca. 398 eV), and oxidized N atoms (ca. 403 eV). Furthermore, four types of O-containing species were present on the surfaces of the microporous PAMBZ-A and PAEBZ-A: quinone (ca. 531.3 eV), adsorbed H₂O (ca. 535.9 eV), C=O (ca. 532.3 eV), and C–OH (ca. 534.2 eV), as presented in Table S1 [7, 43, 44]. The calculated N atom contents were 2.3 wt% for PAMBZ-A and 4.2 wt% for PAEBZ-A. Therefore, we expected these materials to have great potential for application in CO₂ capture. FTIR spectra of PAMBZ-A and PAEBZ-A (Fig. 11) revealed two characteristic peaks at 1350 cm⁻¹ (D band), representing imperfect and disarrayed structures, and 1599 cm⁻¹ (G band), representing the

vibrations of sp²-hybridized carbon atoms [54, 56, 57]. The ratios of the intensities of these signals (I_D/I_G) for PAMBZ-A and PAEBZ-A were 1.2 and 0.97, respectively, suggesting that PAEBZ-A possessed a more regular microporous structure and a lower degree of graphitization [51]. Figures 12a and b display equilibrium CO₂ isotherms of the microporous carbon materials PAMBZ-A and PAEBZ-A, recorded at 298 and 273 K, respectively. The degrees of CO₂ capture of PAMBZ-A at 298 and 273 K were 3.63 and 4.60 mmol g⁻¹, respectively; for PAEBZ-A, these values were 5.53 and 7.20 mmol g⁻¹, respectively. Thus, both PAMBZ-A and PAEBZ-A, after

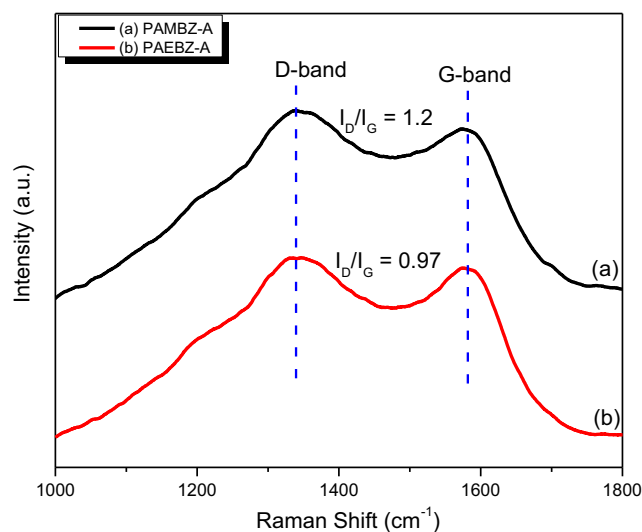
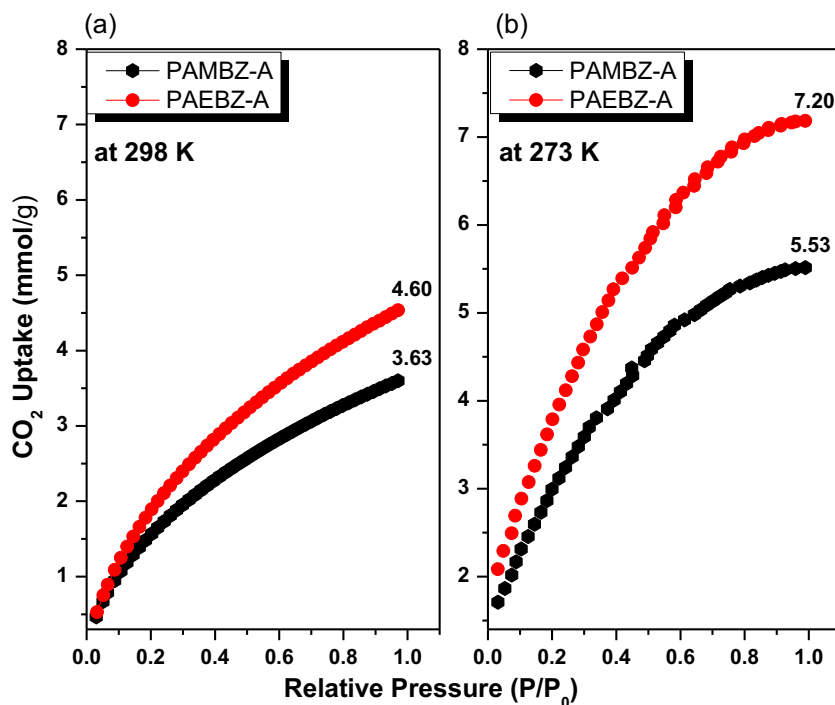


Fig. 11 Raman spectra of PAMBZ-A and PAEBZ-A

Fig. 12 CO₂ uptake profiles of PAMBZ-A and PAEBZ-A, recorded at (a) 298 and (b) 273 K



KOH activation, were microporous carbon materials having excellent CO₂ capture abilities, presumably because of their high surface areas and high N atom contents (pyridonic, pyridinic) enhanced their affinities toward acidic CO₂ gas. Also, PAEBZ-A has higher pore volume, BET surface area, N-atom content, and CO₂ capture capability than that of PAEMZ-A which is assigned to the presence of a more regular microporous structure and a lower degree of graphitization in

PAEBZ-A. Furthermore, the CO₂ capture abilities of PAMBZ-A and PAEBZ-A were higher than those (Table 2) of other types of N-enriched carbon materials derived from PBZs and measured at the same temperatures (298 and 273 K) [53–59].

Table 2 CO₂ uptake performance of PAMBZ-A and PAEBZ-A and other N-enriched porous carbon materials derived from other PBZ matrices

Samples	CO ₂ uptake (mmole/g)		Ref
	298 K	273 K	
PAMBZ-A	3.63	5.53	This work
PAEBZ-A	4.60	7.20	This work
BZPh-A	1.44	–	43
BZCN-A	2.82	–	43
HCM-DAH-1	3.30	–	45
ELF6	3.29	5.82	48
ELF46	2.46	4.14	48
ELF56	2.98	5.27	48
RLF-500	3.13	–	49
BPOP-1	0.98	1.79	50
BPOP-1	0.67	1.45	50
AT-F2–900	3.17	–	41
NPC-1	3.95	6.2	44

Conclusions

We have prepared two types of N-doped microporous carbon matrices, PAMBZ-A and PAEBZ-A, through ROP of the monomers AMBZ and AEBZ and subsequent carbonization and KOH activation. DSC revealed that the thermal curing peaks of AMBZ and AEBZ appeared at lower temperatures than that of the typical Pa-type benzoxazine monomer, presumably because of the azobenzene and COOH groups in these monomers acted as promoters for the ROPs of their benzoxazine units. After thermal curing at 210 and 250 °C, the glass transition temperatures (T_g) and thermal stabilities of both PAMBZ and PAEBZ increased, due to their higher crosslinking densities. Nitrogen gas adsorption/desorption analyses, WXR, TGA, and equilibrium CO₂ isotherms revealed that PAMBZ-A and PAEBZ-A both had high surface areas, microporous and graphitic structures, high thermal stabilities, and excellent CO₂ capture abilities. Furthermore, their CO₂ uptake abilities were greater than those of other previously reported N-doped carbon materials synthesized from other PBZ matrices. Thus, azobenzene-functionalized PBZ matrices appear to be useful materials for CO₂ adsorption and, potentially, for energy storage and other applications.

Compliance with ethical standards

Conflict of interest The authors declare they have no conflicts of interest.

References

- Wang G, Leus K, Zhao S, Voort PVD (2018) Newly designed covalent Triazine framework based on novel N-Heteroaromatic building blocks for efficient CO₂ and H₂ capture and storage. *ACS Appl Mater Interfaces* 10:1244–1249
- Wang Q, Luo J, Zhong Z, Borgna A (2011) CO₂ capture by solid adsorbents and their applications: current status and new trends. *Energy Environ Sci* 4:42–55
- Ahmed, D. S., El-Hiti, G. A.; Yousif, E., Ali, A. A., and Hamed, A. S. (2018). Design and synthesis of porous polymeric materials and their applications in gas capture and storage: a review 25, 75
- EL-Mahdy AFM, Kuo CH, Alshehri A, Young C, Yamauchi Y, Kim J, Kuo SW (2018) Strategic design of triphenylamine- and triphenyltriazine-based two-dimensional covalent organic frameworks for CO₂ uptake and energy storage. *J Mater Chem A* 6: 19532–19541
- Adeniran B, Masika E, Mokaya RA (2014) Family of microporous carbons prepared via a simple metal salt carbonization route with high selectivity for exceptional gravimetric and volumetric post-combustion CO₂ capture. *J Mater Chem A* 2:14696–14710
- Rao AB, Rubin ESA (2002) Technical, economic, and environmental assessment of amine-based CO₂ capture Technology for Power Plant Greenhouse gas Control. *Environ Sci Technol* 36: 4467–4475
- Choi S, Gray MML, Jones CW (2011) Amine-tethered solid adsorbents coupling high adsorption capacity and regenerability for CO₂ capture from ambient air. *ChemSusChem*. 4:628–635
- Wang Y, Dong L, Lai G, Wei M, Jiang X, Bai L (2019) Nitrogen-doped hierarchically porous carbons derived from Polybenzoxazine for enhanced Supercapacitor performance. *Nanomaterials* 9:131–140
- Mohamed MG, El-Mahdy AFM, Ahmed MMM, Kuo SW (2019) Direct synthesis of microporous Bicarbazole-based covalent Triazine frameworks for high-performance energy storage and carbon dioxide uptake. *ChemPlusChem* 84:1767–1774
- Dutta S, Bhaumik A, Wu KCW (2014) Hierarchically porous carbon derived from polymers and biomass: effect of interconnected pores on energy applications. *Energy Environ Sci* 7:3574–3592
- Mohamed MG, EL-Mahdy AFM, Takashi Y, Kuo SW (2020) Ultrastable conductive microporous covalent triazine frameworks based on pyrene moieties provide high-performance CO₂ uptake and supercapacitance. *New J Chem* 44:8241–8253
- Wang HL, Yang Y, Liang YY, Robinson JT, Li YG, Jackson A, Cui Y, Dai HJ (2011) Graphene-wrapped sulfur particles as a rechargeable lithium–sulfur battery cathode material with high capacity and cycling stability. *Nano Lett* 11:2644–2647
- Kelly TL, Gao T, Sailor MJ (2011) Carbon and carbon/silicon composites Templated in Rugate filters for the adsorption and detection of organic vapors. *Adv Mater* 3:1776–1781
- EL-Mahdy AFM, Young C, Kim J, You J, Yamauchi Y, Kuo SW (2019) Hollow Microspherical and Microtubular [3+ 3] Carbazole-Based Covalent Organic Frameworks and Their Gas and Energy Storage Applications. *ACS Appl Mater Interfaces* 11:9343–9354
- Fang BZ, Kim JH, Kim MS, Yu JS (2009) Ordered hierarchical nanostructured carbon as a highly efficient cathode catalyst support in proton exchange membrane fuel cell. *Chem Mater* 21:789–796
- EL-Mahdy AFM, Liu TE, Kuo SW (2020) Direct Synthesis of Nitrogen-Doped Mesoporous Carbons from Triazine-Functionalized Resol for CO₂ Uptake and Highly Efficient Removal of Dyes. *J Hazard Mater* 391:122163
- Lee J, Kim J, Hyeon T (2006) Recent Progress in the synthesis of porous carbon materials. *Adv Mater* 18:2073–2094
- Xu S, Luo Y, Tan B (2013) Recent development of hypercrosslinked microporous organic polymers. *Macromol Rapid Commun* 34:471–484
- Niu W, Li L, Liu X, Wang N, Liu J, Zhou W, Tang Z, Chen S (2015) Mesoporous N-doped carbons prepared with thermally removable nanoparticle templates: an efficient Electrocatalyst for oxygen reduction reaction. *J Am Chem Soc* 137:5555–5562
- Meng Y, Gu D, Zhang F, Shi Y, Yang H, Li Z, Yu C, Tu B, Zhao D (2005) Ordered mesoporous polymers and homologous carbon frameworks: amphiphilic surfactant templating and direct transformation. *Angew Chem Int Ed* 44:7053–7059
- Kou J, Sun LB (2016) Nitrogen-doped porous carbons derived from carbonization of a nitrogen-containing polymer: efficient adsorbents for selective CO₂ capture. *Ind Eng Chem Res* 55:10916–10925
- Casco ME, Kirchhoff S, Leistenschneider D, Rauche M, Brunner E, Borchardt L (2019) Mechanochemical synthesis of N-doped porous carbon at room temperature. *Nanoscale* 11:4712–4718
- Xu S, He J, Jin S, Tan B (2018) Heteroatom-rich porous organic polymers constructed by benzoxazine linkage with high carbon dioxide adsorption affinity. *J Colloid Interface Sci* 509:457–462
- Cui X, Yang Q, Xiong Y, Bao Z, Xing H, Dai S (2017) Preparation of ordered N-doped mesoporous carbon materials via a polymeric liquid assembly. *Chem Commun* 53:4915–4918
- Chu WC, Bastakoti BP, Kaneti YV, Li JG, Yamauchi Y, Alamri HR, Allothman ZA, Kuo SW (2017) Tailored Design of Bicontinuous Gyroid Mesoporous Carbon and Nitrogen-Doped Carbon from Poly (ethylene oxide-*b*-caprolactone) Diblock Copolymers. *Chem Eur J* 23:13734–13741
- Li JG, Ho YF, Ahmed MMM, Liang HC, Kuo SW (2019) Mesoporous Carbons Templated by PEO-PCL Block Copolymers as Electrode Materials for Supercapacitors. *Chem Eur J* 25:10456–10463
- Mohamed MG, Kuo SW (2020) Crown ether-functionalized Polybenzoxazine for metal ion adsorption. *Macromolecules* 2020(53):2420–2429
- Zhang K, Han L, Froimowicz P, Ishida H (2017) Smart latent catalyst containing *o*-trifluoroacetamide functional benzoxazine: precursor for low temperature formation of very high performance polybenzoxazole with low dielectric constant and high thermal stability. *Macromolecules* 50:6552–6560
- Mohamed MG, Kuo SW (2019) Functional silica and carbon Nanocomposites based on Polybenzoxazines. *Macromol Chem Phys* 220:1800306
- Zhang K, Liu Y, Ishida H (2019) Polymerization of an AB-type Benzoxazine monomer toward different Polybenzoxazine networks: when Diels–Alder reaction meets Benzoxazine chemistry in a single-component resin. *Macromolecules* 52:7386–7395
- Lin RC, Mohamed MG, Kuo SW Benzoxazine/Triphenylamine-Based Dendrimers Prepared through Facile One-Pot Mannich Condensations. *Macromol Rapid Commun* 38:1700251
- Lin RC, Kuo SW (2018) Well-defined benzoxazine/triphenylamine-based hyperbranched polymers with controlled degree of branching. *RSC Adv* 8:13592–13611
- Muthukaruppan A, Arumugam H, Krishnan S, Kannan K, Chavali MA (2018) Low cure thermo active polymerization of chalcone based benzoxazine and cross linkable olefin blends. *J Polym Res* 25:163
- Chen WC, Kuo SW (2018) Ortho-imide and Allyl groups effect on highly thermally stable Polybenzoxazine/double-Decker-shaped

- polyhedral Silsesquioxane hybrids. *Macromolecules* 51:9602–9612
35. Kuo SW, Wu YC, Wang CF, Jeong KU (2009) Preparation low surface energy polymer materials by minimizing intermolecular hydrogen bonding interaction. *J Phys Chem C* 113:20666–20673
 36. Liao YT, Lin YC, Kuo SW (2017) Highly thermally stable, transparent, and flexible Polybenzoxazine Nanocomposites by combination of double-Decker-shaped polyhedral Silsesquioxanes and Polydimethylsiloxane. *Macromolecules* 50:5739–5747
 37. Liu N, Li L, Wang L, Zhang S (2017) Organic-inorganic polybenzoxazine copolymers with double decker silsesquioxanes in the main chains: synthesis and thermally activated ring-opening polymerization behavior. *Polymer* 109:254–265
 38. Zhang R, Lu X, Lou C, Zhou C, Xin Z (2019) Preparation of diamine-based polybenzoxazine coating for corrosion protection on mild steel. *J Polym Res* 26:29
 39. Zhang K, Yu X, Wang Y, Liu Y (2019) Thermally activated structural changes of a Norbornene–Benzoxazine–Phthalonitrile thermosetting system: simple synthesis, self-catalyzed polymerization, and outstanding flame Retardancy. *ACS Appl Polym Mater* 1: 2713–2722
 40. Mohamed MG, Lin RC, Tu JH, Lu FH, Hong JL, Jeong KU, Wang CF, Kuo SW (2015) Thermal property of an aggregation-induced emission fluorophore that forms metal–ligand complexes with Zn (ClO₄)₂ of salicylaldehyde azine-functionalized polybenzoxazine. *RSC Adv* 5:65635–65645
 41. Arslan M, Kiskan B, Yagci Y (2018) Benzoxazine-based thermoset with autonomous self-healing and shape recovery. *Macromolecules* 51:10095–10103
 42. Aly KI, Mohamed MG, Younis O, Mahross MH, Hakim MA, Sayed MM (2020) Salicylaldehyde azine-functionalized polybenzoxazine: synthesis, characterization, and its nanocomposites as coatings for inhibiting the mild steel corrosion. *Prog Org Coat* 138:105385–105395
 43. Zhou C, Tao M, Liu J, Liu T, Lu X, Xin Z (2019) Effects of interfacial interaction on corrosion resistance of Polybenzoxazine/SiO₂ Nanocomposite coatings. *ACS Appl Polym Mater* 1:381–391
 44. Araz CR, Ishida H, Maurer FH (2014) Quantifying dispersion in Graphene oxide/reactive Benzoxazine monomer Nanocomposites. *Macromolecules* 47:3685–3692
 45. Mohamed MG, Hsu KC, Kuo SW (2015) Bifunctional polybenzoxazine nanocomposites containing photo-crosslinkable coumarin units and pyrene units capable of dispersing single-walled carbon nanotubes. *Polym Chem* 6:2423–2433
 46. Zhang J, Zhang W, Han M, Pang J, Xiang Y, Cao G, Yang Y (2018) Synthesis of nitrogen-doped polymeric resin-derived porous carbon for high performance supercapacitors. *Microporous Mesoporous Mater* 270:204–210
 47. Mohamed MG, Hsiao CH, Luo F, Dai L, Kuo SW (2015) Multifunctional polybenzoxazine nanocomposites containing photoresponsive azobenzene units. *Catalytic carboxylic acid groups, and pyrene units capable of dispersing carbon nanotubes.* *RSC Adv* 5:45201–45212
 48. Zhang K, Liu Y, Evans CJ, Yang H (2020) Easily Processable thermosets with outstanding performance via smart twisted small-molecule Benzoxazines. *Macromol Chem Phys* 41:1900625–1900630
 49. Zhang K, Yu X, Kuo SW (2019) Outstanding dielectric and thermal properties of main chain-type poly (benzoxazine-co-imide-co-siloxane)-based cross-linked networks. *Polym Chem* 10:2387–2396
 50. Mohamed MG, Kuo SW (2016) Polybenzoxazine/polyhedral Oligomeric Silsesquioxane (POSS) Nanocomposites. *Polymers* 8: 225
 51. Konnola R, Anirudhan TS (2020) Efficient carbon dioxide capture by nitrogen and sulfur dual-doped mesoporous carbon spheres from polybenzoxazines synthesized by a simple strategy. *J Environ Chem Eng* 8:103614–103624
 52. Mohamed MG, Tsai MY, Su WC, EL-Mahdy AFM, Wang CF, Huang CF, Dai L, Chen T, Kuo SW (2020) Nitrogen-doped microporous carbons derived from azobenzene and nitrile-functionalized polybenzoxazines for CO₂ uptake. *Mater Today Commun* 24: 101111
 53. Wu JY, Mohamed MG, Kuo SW (2017) Directly synthesized nitrogen-doped microporous carbons from polybenzoxazine resins for carbon dioxide capture. *Polym Chem* 8:5481–5489
 54. Wan L, Wang J, Sun Y, Feng C, Li K (2015) Polybenzoxazine-based nitrogen-containing porous carbons for high-performance supercapacitor electrodes and carbon dioxide capture. *RSC Adv* 5:5331–5342
 55. Hao GP, Li WC, Qian D, Wang GH, Zhang WP, Zhang T, Wang AQ, Schuth F, Bongard HJ, Lu AH (2011) Structurally designed synthesis of mechanically stable poly(benzoxazine-co-resol)-based porous carbon monoliths and their application as high-performance CO₂ capture sorbents. *J Am Chem Soc* 113:11378–11388
 56. Liu Y, Cao L, Luo J, Peng Y, Ji Q, Dai J, Zhu J, Liu X (2019) Biobased nitrogen- and oxygen-Codoped carbon materials for high-performance Supercapacitor. *ACS Sustain Chem Eng* 7:2763–2773
 57. Shi W, Zhang X, Ji Y, Zhao Z, Li W, Jia X (2019) Sustainable preparation of bio-based Polybenzoxazine resins from amino acid and their application in CO₂ adsorption. *ACS Sustain Chem Eng* 7: 17313–17324
 58. Hao GP, Li WC, Qian D, Lu AH (2010) Rapid synthesis of nitrogen-doped porous carbon monolith for CO₂ capture. *Adv Mater* 22:853–857
 59. Sun X, Li J, Wang W, Ma Q (2018) Constructing benzoxazine-containing porous organic polymers for carbon dioxide and hydrogen sorption. *Eur Polym J* 107:89–95

Publisher's note Springer Nature remains neutral with regard to jurisdictional claims in published maps and institutional affiliations.

Journal of Polymer Research is a copyright of Springer, 2020. All Rights Reserved.